

# Unveiling the Structure of Galaxy Clusters with Combined ESO-VLT, WFI, and XMM-Newton Observations

Hans Böhringer<sup>1</sup>  
 Filiberto Braglia<sup>1</sup>  
 Daniele Pierini<sup>1</sup>  
 Andrea Biviano<sup>2</sup>  
 Peter Schuecker<sup>1</sup>  
 Yu-Ying Zhang<sup>1</sup>  
 Alexis Finoguenov<sup>1</sup>  
 Gabriel W. Pratt<sup>1</sup>  
 Hernan Quintana<sup>3</sup>  
 Paul D. Lynam<sup>4</sup>

<sup>1</sup> Max-Planck-Institut für Extraterrestrische Physik, Garching, Germany

<sup>2</sup> INAF-Osservatorio Astronomico di Trieste, Trieste, Italy

<sup>3</sup> Pontificia Universidad Católica de Chile, Santiago, Chile

<sup>4</sup> ESO

Understanding the dynamical structure and matter content of galaxy clusters is crucial for many cosmological and astrophysical applications. While optical studies provide information on the distribution and dynamics of the galaxies, allowing for a tentative reconstruction of the cluster mass distribution, X-ray observations provide complementary details through the study of the hot, X-ray luminous intracluster plasma which is confined by the cluster's gravitational potential well. To exploit the advantage of such a combined approach we have been conducting observations with VIMOS at the ESO-VLT, the Wide Field Imager at the 2.2-m MPG/ESO telescope at La Silla, and ESA's XMM-Newton X-ray observatory. In this article we illustrate the power of the combination of these instruments for galaxy cluster studies.

Galaxy clusters are important astrophysical laboratories and test objects for cosmological research. The key for this application of galaxy cluster research is the knowledge of the cluster mass and dynamical structure. For instance, the cluster abundance and the statistics of the cluster spatial distribution provide the basis for tests of cosmological models (Böhringer et al. 1998; Schuecker et al. 2003). Among many possible applications, the use of galaxy clusters as laboratories involves (i) the determination of the baryon-to-dark matter ratio, where-

by the clusters provide a representative sample of matter of our Universe, and (ii) the determination of the mass-to-light ratio, which is a measure of the efficiency of galaxy formation. It is obvious that the determination of the cluster mass and internal mass distribution is an essential prerequisite in such studies.

Cluster-mass measurements have so far preferentially been performed on presumably relaxed, regular systems. For general cosmological applications we need to know the mass of clusters of any type. To take one crucial example: the mass function of galaxy clusters provides important information on the statistics of the cosmic large-scale structure. It has been suggested on the basis of some simulations that the X-ray luminosity, the X-ray temperature, and the galaxy velocity dispersion, all three important indicators of the cluster mass, may be boosted to high values during major mergers of galaxy clusters. Thus, in many important surveys, where these measures of cluster mass have been used without this precaution, the high end of the mass function could be seriously distorted, thereby leading to incorrect implications. This and other important applications, which rely on a precise knowledge of cluster structure and mass, have led us to embark on a systematic study of cluster structure for representative cluster samples using detailed observations at X-ray and optical wavelengths.

While deep X-ray images, which show the distribution of the hot intracluster medium (ICM) tracing the gravitational potential of the cluster, reveal much of the cluster structure as projected onto the sky, the galaxy redshift distribution provides a complementary view of the cluster dynamics projected onto the line-of-sight. Thus, a major aim of the project is to employ the combined X-ray/optical information for the reconstruction of the dynamical state of the cluster, to search for the best strategy for the mass estimate for each case, and to test the consistency of the optical and X-ray mass estimates. For this research Europe currently offers two superb instruments. The XMM-Newton X-ray observatory with its high throughput, good spatial resolution (8 arcsec), and simultaneous imaging and spectroscopic capabilities is by far

the best instrument to study the density, temperature, pressure and entropy structure of the ICM. This provides a very good basis for mass estimates as well as an understanding of the formation and thermal history of the cluster and its ICM. The VIMOS multiplexing spectrograph at the ESO-VLT is the most efficient instrument (apart from IMACS at Magellan) to collect sufficient numbers of redshifts for a dynamical analysis. In addition the Wide Field Imager (WFI) allows us to map the optical emission from the cluster galaxies on large scales. Further goals of this programme involve the study of the galaxy population and the star-formation activity as a function of environment in and around the cluster, the relation of the heavy element abundances in the ICM with the properties of the galaxy population, and the connection between the thermal structure of the ICM and the galaxy distribution and dynamics (which can provide clues on the accretion history of the cluster).

While we have already collected interesting results on the X-ray and optical properties of the clusters in this project, the overall data assessment and interpretation are still in progress. Here we would therefore like to give an illustration of the diagnostic power of the combined use of VLT-VIMOS and XMM-Newton observations, in particular, and to describe our observational approach.

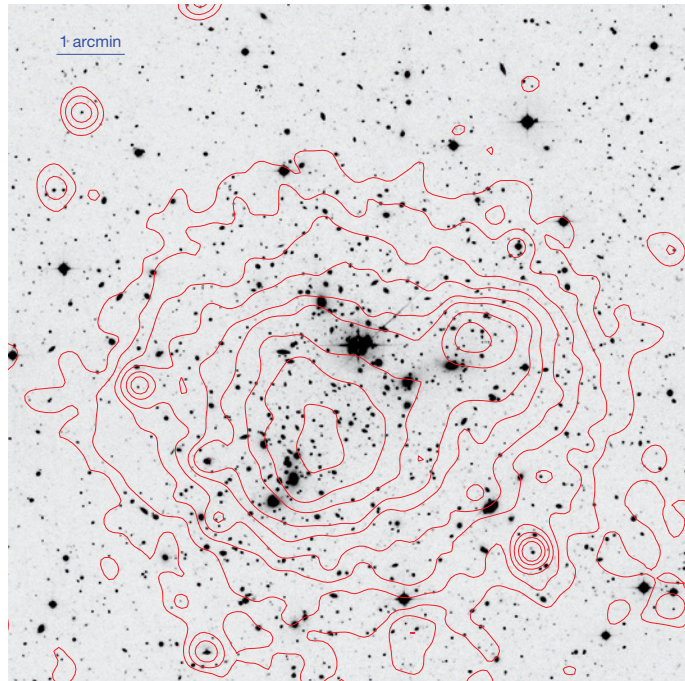
## X-ray morphology

As an example of this diagnostic power we choose the case of the massive cluster RXCJ 0014.3-3023 (Abell 2744), reproduced in a composite colour WFI image in Figure 1. This cluster is taken from our complete sample of massive galaxy clusters (with X-ray luminosity above  $2 \cdot 10^{45} h_{50}^{-1} \text{ erg s}^{-1}$  for 0.1–2.4 keV) in the redshift range from  $z = 0.27$  to 0.31 in the southern sky, as identified in our ROSAT Sky Survey-based REFLEX Cluster Survey (Böhringer et al. 1998, 2004). The X-ray-determined mass of the cluster is about  $7.4 \cdot 10^{14} h_{70}^{-1} M_{\odot}$  inside a radius  $1.24 h_{70}^{-1} \text{ Mpc}$  (i.e. half of the virial radius), excluding substructure (Zhang et al. 2006). This cluster is also known as a gravitational lens (Smail et al. 1991). An overlay of the X-ray contours (Figure 2)

**Figure 1:** Colour composite image of the cluster RXCJ 0014.3-3023 (A2744) obtained from *B*- (blue, 4800 s exposure), *V*- (green, 3600 s), and *R*-band (red, 3600 s) imaging with the Wide Field Imager at the 2.2-m MPG/ESO telescope at La Silla. The angular size of the field shown is  $10'$  on a side ( $2.7 h_{70}^{-1}$  Mpc for the 'concordance' cosmological model). East is to the left and North up.



**Figure 2:** X-ray contour plot of the 0.5 to 2.0 keV XMM-Newton image superposed on the *R*-band WFI image for RXCJ 0014.3-3023. We clearly see two X-ray maxima tracing the gravitational potential minima of the main cluster (to the SE) and a subcluster (to the NW), both also marked by slightly offset concentrations of massive galaxies.



reveals two X-ray maxima belonging to the main cluster to the South-East (SE) and a considerable subcluster to the North-West (NW), which are in the process of merging.

Two signatures indicate that the NW subcluster is still on its infalling track. Namely: (1) the galaxies are preceding the intra-cluster plasma of the subcluster, which is stopped by the interaction with the main cluster's ICM, and (2) a detailed Chandra X-ray image shows signs of a bow shock in front (i.e. to the SE) of the infalling subcluster (Kempner and David 2004). The latter signature is consistent with an entropy enhancement in the region between the two maxima discovered from our XMM-Newton observations (Figure 3, Finoguenov et al. 2005).

### Galaxy population

To study the galaxy population we covered the region of RXCJ 0014.3-3023 with three VIMOS fields, overlapping at the cluster centre, aligned in the EW direction. For each field (but one), we designed one multi-object spectroscopy (MOS) mask for a few bright galaxies and one MOS mask for many faint galaxies. The total exposure time was about

one hour per field including all overheads. With the VIMOS Low-Resolution Blue grism and a conservative 3 arcsec-wide sky strip per slit, we obtained in total 871 spectra including 134 confirmed cluster members. The targets were selected from an *I*-band image with no colour selection to obtain an unbiased view of the galaxy population as a function of star-formation activity. The MOS masks cover the entire cluster slightly beyond the virial radius ( $\sim 2.5 h_{70}^{-1}$  Mpc), where the cluster galaxy density becomes low. Thus, the investment for covering this important outer region is a reduction in the overall efficiency.

Figure 4 shows typical galaxy spectra. At the dispersion given by the coupling of the low-resolution grism (a price paid for the high multiplexing power of VIMOS) with the 1-arcsec-wide slits adopted, the galaxy velocities have relatively large uncertainties (of the order of  $300 \text{ km s}^{-1}$ ) and the sensitivity for the detection of emission lines is reduced with respect to higher-resolution spectroscopy. However, as we show below, we still obtain much useful information. The sensitivity limit for the detection of emission lines still corresponds to about  $10 \text{ \AA}$  in equivalent width. Since one of our goals is the study of the nature of the galaxy population

as a function of environment, we show in Figure 5 (left hand) as an example the cumulative ratio of emission-line galaxies versus galaxies with spectra typical of passive stellar populations. We clearly see an increase in star-formation activity at larger cluster radii which has been seen before (e.g. Kodama et al. 2001) and in the Sloan Digital Sky Survey in nearby clusters (Gomez et al. 2003). There is a very clear signature that star formation is quenched inside the cluster and this quenching sets in far outside the virial radius. This implies that the interaction with the hot cluster ICM (e.g. by interstellar gas stripping effects) is not the only mechanism that leads to a suppression of star formation in cluster galaxies. Quenching effects must already be operative in the infall region. The actual projected distributions of star-forming and non-star-forming galaxies in the cluster are shown in Figure 5 (right hand). There is no obvious correlation between the distribution of emission-line galaxies and the merger structure of the cluster. Also, we note that most of the emission-line galaxies are found at large radii, except for a striking compact group of three emission-line objects near the cluster centre, which could well lay off-centre along the line-of-sight.

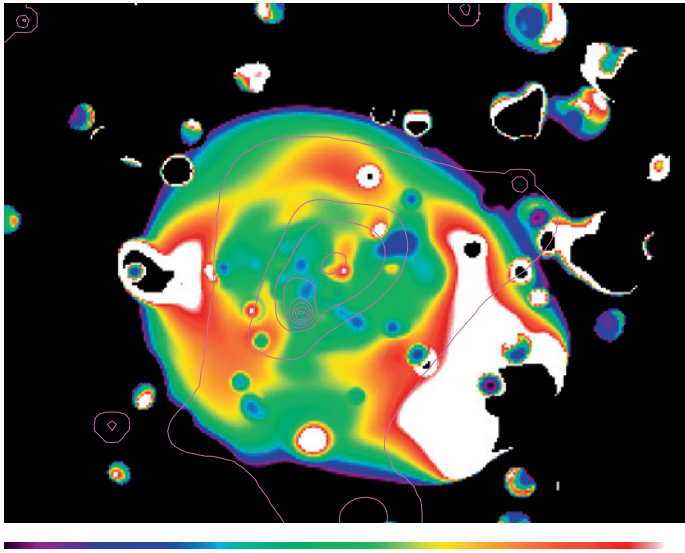


**Figure 3 (above):** Entropy structure of the ICM in RXCJ 0014.3-3023 seen in projection as derived from the XMM-Newton spectro-imaging (Finoguenov et al. 2005). While we expect the entropy to steadily increase with radius in a relaxed cluster, we here observe low entropy gas (in blue) marking the two subcomponent centres, whereas the high entropy (in yellow/red) in the region in-between implies energy dissipation due to the merger shock. Another interesting feature is the low-entropy channel connecting the main cluster centre with the southern edge (in green). The overplotted contours show the galaxy distribution (see Figure 7).

**Figure 5 (below):** Left: Radial distribution of the cumulative ratio of galaxies with and without emission lines in their spectra. The central peak in the blue line (all galaxies) is due to only three galaxies (see right hand), which are excised in the red curve. Right: Projected distribution of the galaxies with spectroscopic observations. Different colours mark the redshift regions (blue:  $\Delta v < -1321$  km s<sup>-1</sup>, green:  $-1321 < \Delta v < 0$  km s<sup>-1</sup>, yellow:  $0 < \Delta v < 1321$  km s<sup>-1</sup>, red:  $\Delta v > 1321$  km s<sup>-1</sup>) and the asterisk symbol indicates ongoing star formation activity. The cluster centre is marked by a cross.

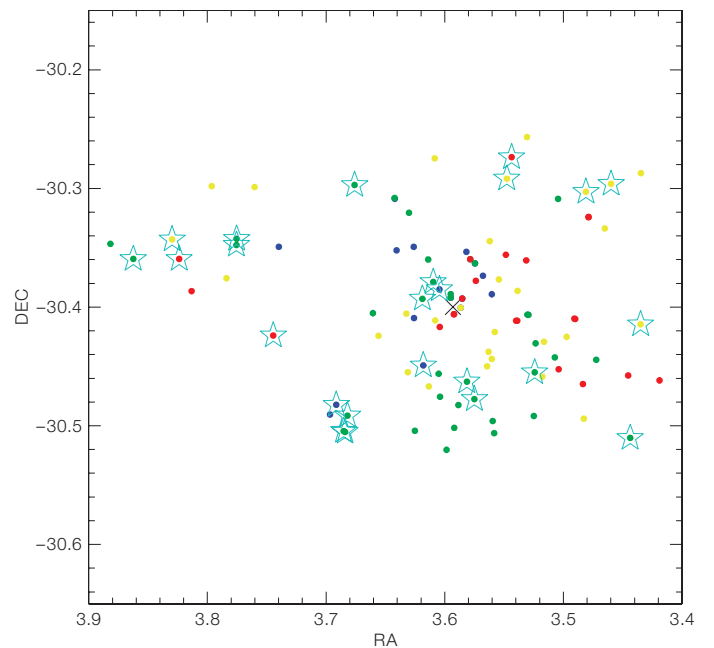
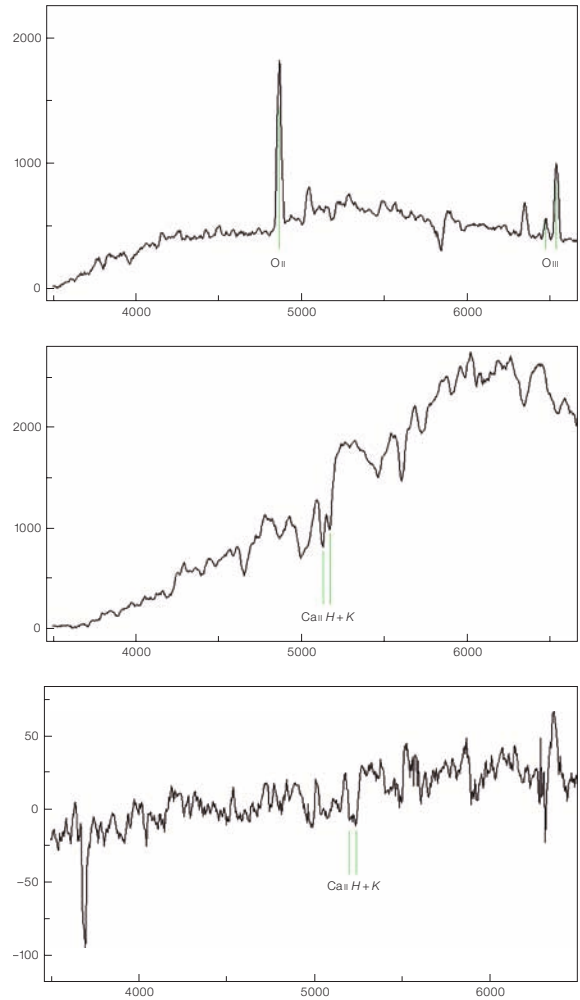
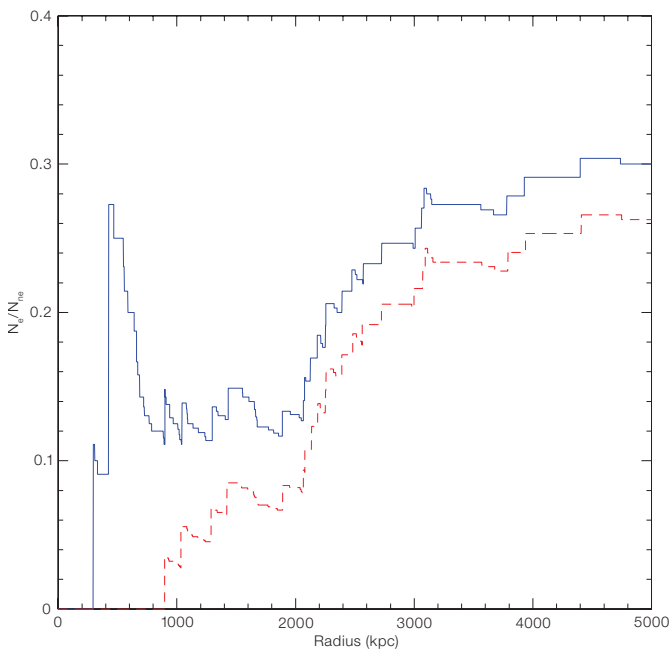
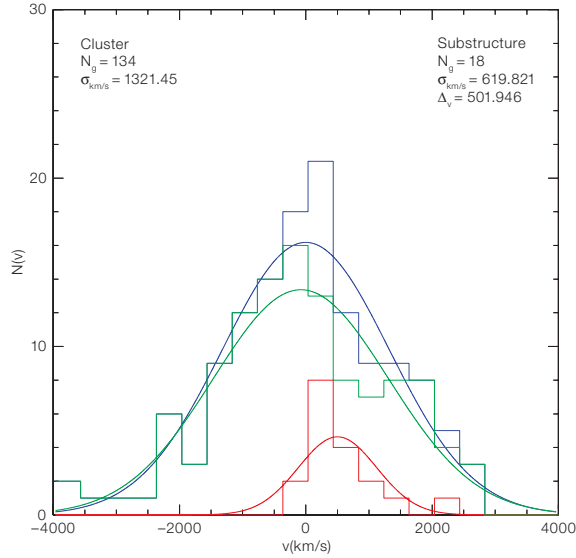


**Figure 4:** Examples of VIMOS spectra (observed-frame wavelength in Å) of three cluster galaxies, including a star-forming emission-line galaxy (top) and two galaxies dominated by old, passively evolving stellar populations (middle and bottom). While the upper two examples include two bright galaxies, a galaxy near the detection limit of 22.5 I-mag is shown at the bottom.

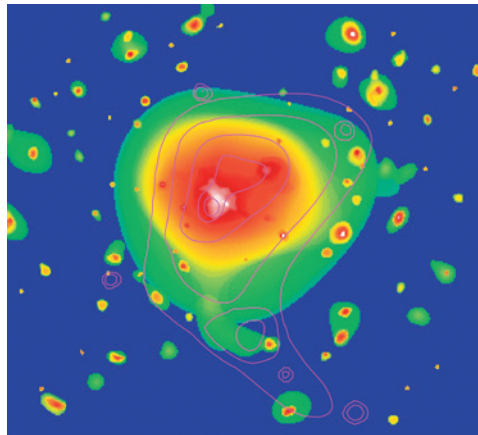
### The structure of the cluster merger

Figure 6 shows the (rest-frame) velocity distribution of the galaxies in the cluster. The overall velocity dispersion is very large, with  $\sigma_v = 1321 \text{ km s}^{-1}$ . Since there is a clear signature of an infalling subcluster in X-rays, we can use this information to search for a velocity difference between the two subcomponents. Therefore Figure 6 also shows the velocity distribution of the galaxies in the region to the right and above a point intermediate to the two X-ray maxima. This section nicely separates the infalling subcluster from the main cluster. We note a clear shift to higher velocities for the infalling subcluster, with a mean velocity difference of about  $500 \text{ km s}^{-1}$ . Since we see clear signatures in X-rays that the two subcomponents are interacting (e.g. a high entropy region in the X-ray emitting plasma between the two X-ray maxima, see Figure 3), we interpret the higher redshift of the subcluster as indicating that this subcomponent is infalling from the front. We can further speculate that the mutual attraction of the two subcomponents with a combined mass of about  $10^{15} h_{70}^{-1} M_\odot$  allows a maximum approach velocity at a separation of about 1 Mpc (equivalent to a separation of about  $800 h_{70}^{-1} \text{ kpc}$  in projection) of about  $2200 \text{ km s}^{-1}$ . The low observed line-of-sight velocity thus implies that the merger axis is near the plane of the sky with an angle of the order of about 15 degrees. The signature of a bow shock seen in the Chandra data (Kempner and David 2004) supports this picture of a motion almost perpendicular to the line-of-sight. A more detailed analysis of this merger structure is in progress, and we also plan to support our investigation by comparison to tailored simulations.

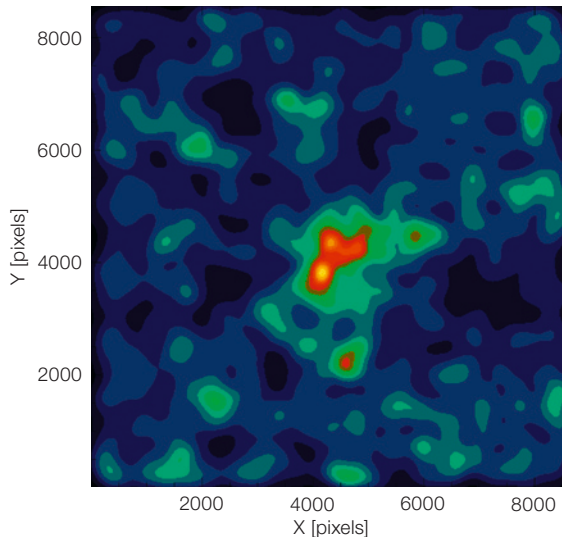
The strategy we then adopted for the mass analysis of the cluster is to use the undisturbed sector of the main cluster (see Zhang et al. 2006). Both the spectroscopic dynamical analysis and the X-ray analysis were then performed excluding the substructure. Our assumption of a relatively undisturbed sector of the cluster is supported by the fact that we observe a gently falling velocity dispersion profile in this sector, as expected for a regular cluster. Preliminary results based on the sky and velocity distribution of the galax-



**Figure 6:** Histogram and Gaussian fit of the RXCJ 0014.3-3023 galaxy velocity distribution from the VIMOS spectroscopic observations. The blue curves show the overall distribution, while the red curves give the distribution of galaxies in the sector covered by the infalling subcluster, showing a higher recession velocity by about  $500 \text{ km s}^{-1}$ . The green curves show the velocity distribution of the remaining galaxies.



**Figure 7:** Projected distribution of galaxies with  $R \leq 22 \text{ mag}$  (without z-cut) in the cluster RXCJ 0014.3-3023 and its surroundings. **Top:** The X-ray surface brightness map with the galaxy number density superposed as a contour plot. Colours from white to green correspond to decreasing X-ray surface brightnesses. The maximum of the galaxy distribution clearly marks the centre of the main cluster. In the outer contours we recognise extensions to the NW and to the S. **Bottom:** The galaxy distribution on scale that is twice as large (entire WFI field-of-view) and to lower overdensity thresholds (decreasing from yellow to black). The extensions of the top panel now find their continuation in possible filaments of galaxy overdensities leading further away from the cluster.



ies give a value for the mass of the main cluster that is in agreement with the X-ray estimate.

### The surroundings

The large field-of-view of the WFI camera ( $34' \times 33'$ ) allows us to image the whole cluster together with its infall region. Figure 7 (top) shows a contour plot of the projected galaxy density distribution down to  $R \sim 22$  mag (no  $z$ -cut being applied) superposed on the X-ray image, and (bottom) a large-scale map of the galaxy distribution extending even outside the virial radius of RXCJ 0014.3-3023. The maximum of the galaxy density distribution is centred on the main cluster. The extensions in the galaxy distribution and the X-ray surface brightness distribution to the NW and to the South (S) in Figure 7 (top) find their continuation in a possible large-scale filamentary structure in the bottom panel of this figure, where the galaxy distribution is reproduced with a lower threshold for the density contours. There is a very interesting correspondence between the filaments and the internal structure of the cluster, although a spectroscopic confirmation is needed. The main subcluster is falling into the system from the NW. The extension to the S is connected to a low entropy channel linking the possible filament with the cluster centre (Figure 3). We have seen analogous features in other clusters of our sample and we inter-

pret them as the signature of a previous infall of galaxy groups, with a low entropy intergroup medium, from the surrounding large-scale filamentary structure. Thus we are obtaining a glimpse of the accretion history of this cluster. The fact that RXCJ 0014.3-3023 exhibits a giant radio halo (see Kempner and David 2004), which was most probably formed by cosmic-ray acceleration in a previous merger shock, is a further confirmation that this cluster has recently suffered from other mergers in addition to the one observed here.

### Outlook

Similar results to those shown here have been obtained in the past from deep optical and X-ray studies. The point here is that the power of XMM-Newton and VLT-VIMOS makes such observations a routine enterprise which can be applied to a larger, representative sample of galaxy clusters. We are currently exploiting these two facilities to study two representative cluster samples, one comprised of the most massive, southern galaxy clusters in the redshift range from  $z = 0.27$  to  $0.31$ , all observed with XMM-Newton, from which the above example was taken, and for more than half of which we have recently collected VIMOS data. The other sample, covering the whole mass range of clusters in a homogeneous way, was designed from the REFLEX sample in the redshift range from  $z = 0.055$  to  $0.2$ .

For all 33 clusters of this sample deep XMM-Newton observations have been conducted, and now we inspect a wide spectrum of cluster morphologies. So far only few optical data are available but systematic observations are planned. As spectroscopy at medium redshift and low resolution on a wide field is time-demanding, complements to VIMOS will be considered at no loss of efficiency or science throughput. Both samples are becoming benchmark samples, for which observations based on the Sunyaev Zel'dovich effect are scheduled, and lensing studies are planned. With this rich information on cluster structure we will significantly improve our calibration of cluster mass measurements, as these first results illustrate.

### Acknowledgements

The X-ray data used here are based on observations with XMM-Newton, an ESA science mission with instruments and contributions directly funded by ESA member states and NASA.

### References

- Böhringer, H. et al. 1998, *The Messenger* 94, 21
- Böhringer, H. et al. 2004, *A&A* 425, 367
- Finoguenov, A., Böhringer, H., Zhang, Y.-Y. 2005, *A&A* 442, 827
- Gomez, P. L. et al. 2003, *ApJ* 584, 210
- Kempner, J. C., David, L. P. 2004, *MNRAS* 349, 385
- Kodama, T. et al. 2001, *ApJ* 562, L9
- Schuecker, P., et al. 2003, *A&A* 398, 867
- Smail, I. et al. 1991, *MNRAS*, 252, 19
- Zhang, Y.-Y. et al. 2006, *A&A*, submitted



The centre of the globular cluster Messier 12 as observed with the FORS1 multi-mode instrument on ESO's Very Large Telescope. The picture covers a region of about 3.5 arcmin on a side, corresponding to about 23 light years at the distance of Messier 12. It is based on data in five different filters:  $U$ ,  $B$ ,  $V$ ,  $R$  and  $H\alpha$ . The observations were obtained with very good conditions, the image quality ('seeing') being around 0.6 arcsec. (ESO PR Photo 04/06)